Simulation of the Plasma Generated in a Gas Bubble

Lizhu Tong[1]
[1]Keisoku Engineering System Co., Ltd.
1-9-5 Uchikanda, Chiyoda-ku, Tokyo 101-0047, Japan, tong@kesco.co.jp

Abstract: The plasmas generated in water involve various physical phenomena such as flows agitated by bubbles, high electric fields for breakdown, discharges in bubbles with the size variation, and so on. In this paper, studies have been made on the simulation of plasmas generated in bubbles with the size variation. The species taken in account include electrons, three kinds of ions, and ten kinds of neutral (molecule, radical, excited) species. 43 chemical reactions are considered. The time evolution of bubble size is simulated using the moving mesh method provided in COMSOL Multiphysics. The plasma properties during the variation in bubble size are obtained. The effect of the duration for the variation in bubble size and the maximum bubble size on discharge properties is examined.

Keywords: Gas Bubble, Atmospheric Pressure Plasma, Moving Boundary.

1. Introduction

Electrical discharges in gas-liquid environments and in liquids (primarily water, but in some cases also organic liquids) have been studied for a number of years for applications in electrical transmission, chemical destruction in pollution control, chemical synthesis, polymer surface treatment, biological inactivation, biomedical treatment, material and nanoparticle synthesis, and chemical analysis of liquid solutions [1].

Discharges directly inside bubbles have presented an interesting case for fundamental studies and potential applications because of large surface areas and the presence of the gas phase for ease of discharge initiation [2-5]. Some model simulations for discharges within humid air or injected gas in bubbles have been reported [6-9]. Since the bubble size varies during discharge, the plasma simulation in bubbles becomes complicated. Until now the studies are performed only for either bubble dynamics [6,7] or plasma properties ignoring the variation in bubble size [8,9].

In this work, bubble dynamics and plasma properties are coupled into a one-dimensional (1-D) bubble plasma model. The plasma module and the moving mesh technique provided in COMSOL Multiphysics are used. The plasma properties within bubbles are presented and discussed.

2. Numerical Model

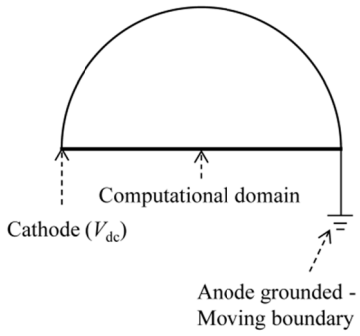

Figure 1. Schematic of 1-D bubble plasma model.

The simulations are performed using 1-D plasma model in a 100%H_2O gas bubble at atmospheric pressure. The bubble radius is varied from 1 to 8.5 mm, which is taken from the previous research on bubble dynamics [7]. The study is made for the first period of the variation in bubble radius [6,7]. The duration for the variation in bubble radius is chosen τ = 0.8, 1.6, or 2.4 ms. The plasma species taken in account include the ions: H_2O^+, O_2^+, H_2^+, the neutrals: H_2O, H, OH, H_2, $O(^1D)$, O, O_2, O_3, HO_2, H_2O_2, as well as electrons. The reactions of electron impact collision and those of ions and neutral species are listed in Table 1. The detailed information for plasma modeling can be found in our previous work [13,14].

1-D bubble plasma model for the plasmas generated in bubbles is shown in Fig. 1. A dc power supplied voltage V and a ballast resistor R_b are used. V_{dc} is discharge voltage and j is discharge current density. V_{dc} is solved by

$$V = V_{dc} + jAR_b, \quad (1)$$

where V= - 1 kV, R_b = 10 kΩ. A is set 0.03 cm^2 in this work.

The moving mesh technique, named as Arbitrary Langrangian Eulerian (ALE) method,

is used to trace the variation in solved domain.

Table 1: The chemical reactions included in the model.

No.	Reaction	Ref.
1	$e^- + H_2O \rightarrow e^- + H_2O$	10
2	$e^- + H_2O \rightarrow e^- + H + OH$	10
3	$e^- + H_2O \rightarrow e^- + H_2 + O(^1D)$	10
4	$e^- + H_2O \rightarrow 2e^- + H_2O^+$	10
5	$e^- + H_2 \rightarrow e^- + H_2$	10
6	$e^- + H_2 \rightarrow e^- + H + H$	10
7	$e^- + H_2 \rightarrow 2e^- + H_2^+$	10
8	$e^- + O_2 \rightarrow e^- + O_2$	11
9	$e^- + O_2 \rightarrow e^- + O + O$	11
10	$e^- + O_2 \rightarrow e^- + O + O(^1D)$	11
11	$e^- + O_2 \rightarrow 2e^- + O_2^+$	11
12	$e^- + O \rightarrow e^- + O(^1D)$	11
13	$O(^1D) \rightarrow O$	12
14	$2O + O_2 \rightarrow O_3 + O$	12
15	$O + 2O_2 \rightarrow O_3 + O_2$	12
16	$H + O + H_2 \rightarrow OH + H_2$	12
17	$H + O + H_2O \rightarrow OH + H_2O$	12
18	$H + O_2 + H_2 \rightarrow HO_2 + H_2$	12
19	$H + O_2 + O_2 \rightarrow HO_2 + O_2$	12
20	$H + O_2 + H_2O \rightarrow HO_2 + H_2O$	12
21	$H + OH + H_2 \rightarrow H_2O + H_2$	12
22	$H + OH + O_2 \rightarrow H_2O + O_2$	12
23	$H + O_3 \rightarrow OH + O_2$	12
24	$H + O_3 \rightarrow O + HO_2$	12
25	$H + HO_2 \rightarrow H_2O + O$	12
26	$H + HO_2 \rightarrow O_2 + H_2$	12
27	$H + HO_2 \rightarrow 2OH$	12
28	$O + O(^1D) \rightarrow 2O$	12
29	$O(^1D) + H_2 \rightarrow OH + H$	12
30	$O(^1D) + O_2 \rightarrow O + O_2$	12
31	$O(^1D) + O_3 \rightarrow 2O_2$	12
32	$O(^1D) + O_3 \rightarrow 2O + O_2$	12
33	$O(^1D) + OH \rightarrow H + O_2$	12
34	$O + HO_2 \rightarrow OH + O_2$	12
35	$O(^1D) + HO_2 \rightarrow OH + O_2$	12
36	$O(^1D) + H_2O_2 \rightarrow H_2O + O_2$	12
37	$O(^1D) + H_2O \rightarrow O + H_2O$	12
38	$O(^1D) + H_2O \rightarrow H_2 + O_2$	12
39	$OH + O_3 \rightarrow HO_2 + O_2$	12
40	$2OH \rightarrow H_2O_2$	12
41	$OH + HO_2 \rightarrow O_2 + H_2O$	12
42	$OH + H_2O_2 \rightarrow H_2O + HO_2$	12
43	$2HO_2 \rightarrow H_2O_2 + O_2$	12

The method enjoys the advantages of both Eulerian and Langrangian frames of reference and can capture the greater deformation with the higher resolution [15]. ALE method comprises of two frames: a reference frame with X coordinate for a 1-D formulation and a spatial frame with x coordinate. The reference frame has fixed coordinates while the spatial frame has coordinates moving with time, subject to boundary conditions. The mesh displacement is obtained by solving the following equation

$$\frac{\partial^2}{\partial X^2}\frac{\partial x}{\partial t} = 0. \qquad (2)$$

3. Results

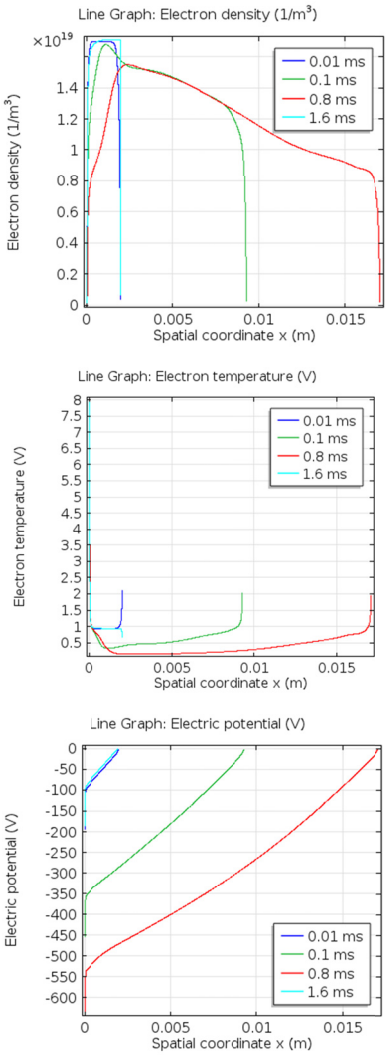

Figure 2. Electron density, electron temperature, and electric potential at the different times for $\tau = 1.6$ ms.

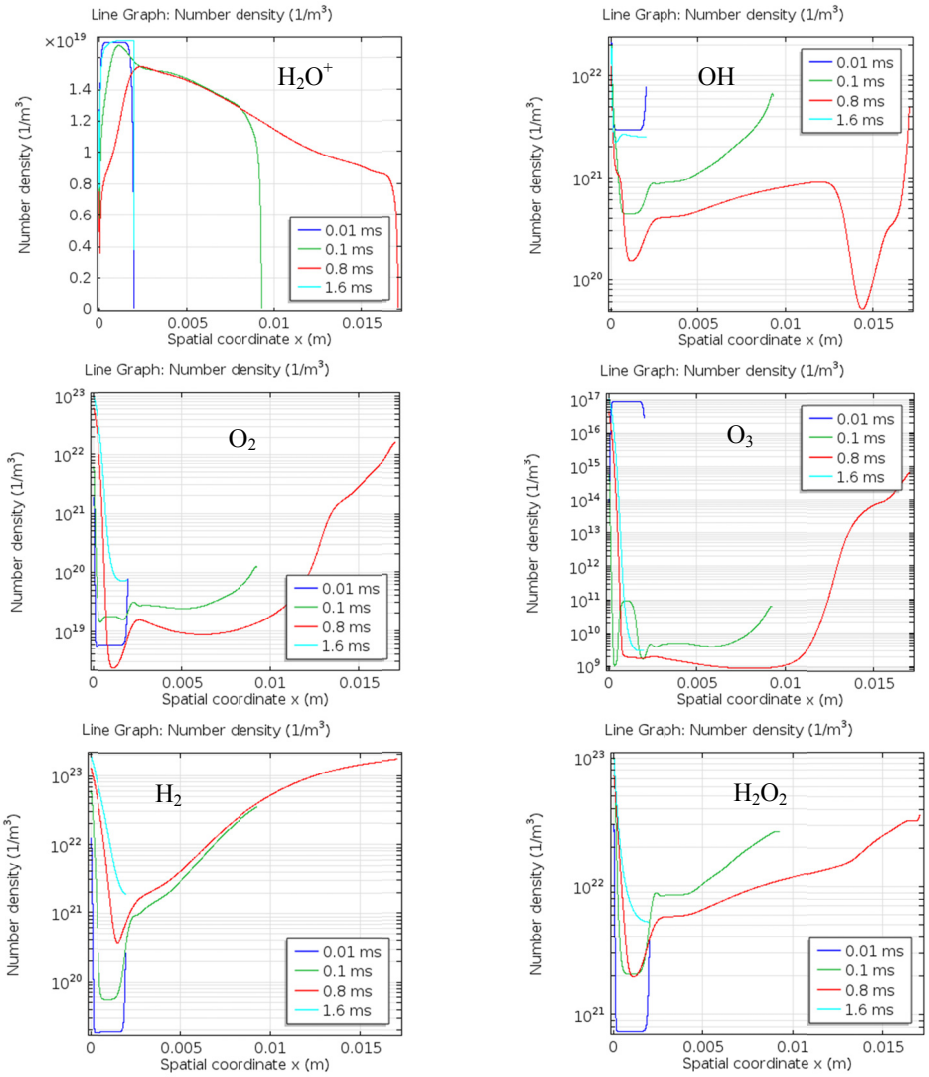

Figure 3. Densities of chemical species at the different times for $\tau = 1.6$ ms.

Figure 2 shows the electron density, electron temperature, and electric potential at the different times for $\tau = 1.6$ ms. As the bubble size is enlarged, the electron density extends from the surface of cathode to anode grounded. At $t = 0.8$ ms, the largest bubble size reaches, in which the electron density in the neighborhood of cathode appears a large reduction. The highest electron temperature is located in the region close to the cathode during the whole discharge, which sustains the behavior of DC discharge.

The density of H_2O^+ ion is shown in Fig. 3. The densities of H_2^+ and O_2^+ ions are found to be two orders lower than H_2O^+, so that both are not presented here. As shown in Fig. 3, the distributions of neutral species have a common aspect, *i.e.*, the high densities appear in the neighborhood of cathode, but as the increase in bubble size, the densities in the region depart from cathode are dramatically reduced over two orders. After $t = 0.8$ ms, due to the reduction of solved domain, the densities start to rise up. The production efficiency of H_2O_2 for discharge inside gas bubble has been reported [2,4]. It is noted that OH radicals play some important roles, such as oxidation, decomposition of organic pollutants, and so on. The densities of H_2O_2 and OH obtained in this work are possessed of a high

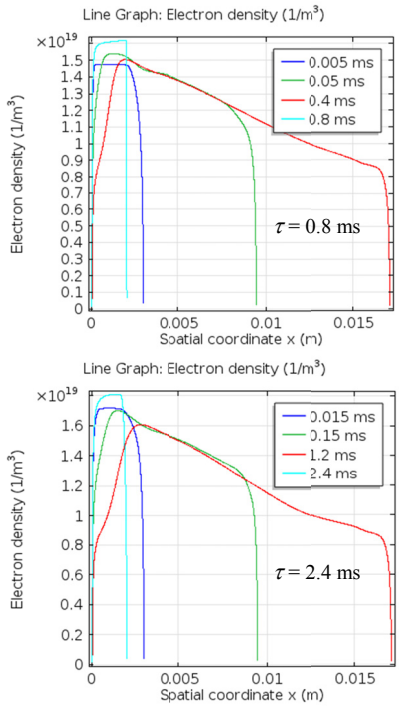

Figure 4. Electron density at the different times for τ = 0.8 and 2.4 ms.

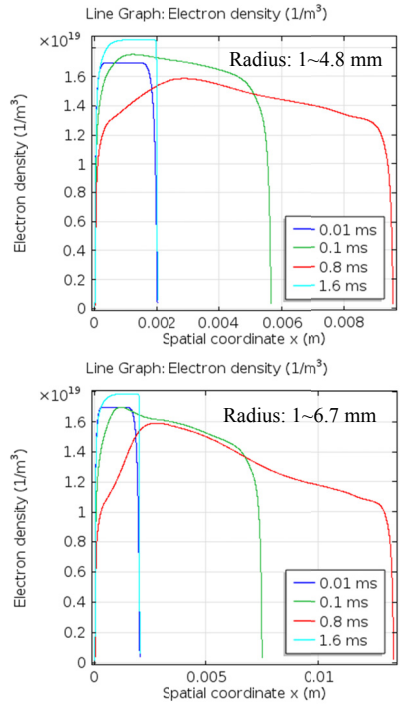

Figure 5. Electron density at the different times for the variations of bubble radius: 1~4.8 and 1~6.7 mm at τ = 1.6 ms.

level values, as shown in Fig. 3. The density of O_3 is found to be five orders lower than other neutral species, which is similar to some previous researches, *e.g.*, the density of O_3 has been reported to be dramatically reduced as the increase of H_2O concentration and the density of O_3 presents a very low value when H_2O concentration rises up to only 6% [9].

Figure 4 shows the results for the duration for the variation in bubble size of 0.8 and 2.4 ms. The electron density at τ = 0.8 ms is distinctly lower than that at τ = 2.4 ms, especially for the time of small bubble size. This could be deduced that longer discharge times cause more ionizations so that the electron density is increased at τ = 2.4 ms. The results for different variations in bubble radius are given in Fig. 5. The bubble radius varies with 1~4.8 and 1~6.7 mm. As the reduction of maximum bubble radius, the electron density becomes relative uniform in the bulk of discharge. The damping phenomenon in the region far from cathode is remitted.

4. Conclusions

The simulation of the plasma generated in a gas bubble is performed using COMSOL Multiphysics 4.3a. The moving mesh technique is coupled for the first time with plasma simulation. The obtained densities of chemical species, such as OH, H_2O_2, and so on, would be beneficial to many further researches on environmental applications.

The present research provides an efficient method to study plasmas generated in bubbles, especially in water.

5. References

1. V.I. Parvulescu, M. Magureanu, P. Lukes, *Plasma Chemistry and Catalysis in Gases and Liquids*, Wiley-VCH Verlag & Co. KGaA, Weinheim, Germany (2012).

2. K.Y. Shih, B.R. Locke, "Effects of electrode protrusion length, pre-existing bubbles, solution conductivity and temperature, on liquid phase pulsed electrical discharge", *Plasma Process. Polym.*, **6** (11), 729–740 (2009).

3. K. Yasuoka, K. Sato, "Development of repetitive pulsed plasmas in gas bubbles for water treatment", *Int. J. Plasma Environ. Sci. Technol.*, **3** (1), 22-27 (2009).

4. L. Němcová, A. Nikiforov, C. Leys, F. Krcma, "Chemical efficiency of H_2O_2 production and decomposition of organic compounds under action of DC underwater discharge in gas bubbles", *IEEE Trans. Plasma Sci.*, **39** (3), 865-870 (2011).

5. M. Kurahashi, S. Katsura, A. Mizuno, "Radical formation due to discharge inside bubble in liquid", *J. Electrostatics*, **42**, 93-105, (1997).

6. J.A. Cook, A.M. Gleeson, R.M. Roberts, "A spark-generated bubble model with semi-empirical mass transport", *J. Acoust. Soc. Am.*, **101** (4), 1908-1920 (1997).

7. X.P. Lu, "One-dimensional bubble model of pulsed discharge in water", *J. Appl. Phys.*, 102, 063302(4pp) (2007).

8. N.Y. Babaeva, M.J. Kushner, "Structure of positive streamers inside gaseous bubbles immersed in liquids", *J. Phys. D: Appl. Phys.*, **42**, 132003 (5pp) (2009).

9. N. Takeuchi, Y. Ishii, K. Yasuoka, "Modelling chemical reactions in dc plasma inside oxygen bubbles in water", *Plasma Sources Sci. Technol.*, **21**, 015006 (8pp) (2012).

10. LXcat, http://www.lxcat.laplace.univ-tlse.fr

11. COMSOL Multiphysics 4.3a- Model library for Plasma Module.

12. D.X. Liu, P. Bruggeman, F. Iza, M.Z. Rong, M.G. Kong, "Global model of low-temperature atmospheric-pressure He+H_2O plasmas", *Plasma Sources Sci. Technol.* **19** (2), 025018 (2010).

13. L.Z. Tong, "Effect of gas flow rate and gas composition in Ar/CH_4 inductively coupled plasmas", *COMSOL Conference 2011 Boston*, USA (2011).

14. L.Z. Tong, "Numerical study of the effect of gas flow in low pressure inductively coupled Ar/N_2 plasmas", *Central European Journal of Physics* **10** (4), 888-897 (2012).

15. K.B. Deshpande, "Validated numerical modelling of galvanic corrosion for couples: Magnesium alloy (AE44)–mild steel and AE44–aluminium alloy (AA6063) in brine solution", *Corrosion Sci.* **52**, 3514–3522 (2010).